Aeroassist Flight Experiment Heating-Rate Sensitivity Study

W. C. Rochelle,* P. C. Ting,† S. A. Bouslog,† S. R. Mueller,‡ and J. E. Colovin Jr.§
Lockheed Engineering & Sciences Company, Houston, Texas 77058
and
D. M. Curry¶ and C. D. Scott**
NASA Johnson Space Center, Houston, Texas 77058

A description of the sensitivities associated with predicting the aerothermodynamic environment on the aeroassist flight experiment (AFE) aerobrake is presented. The objective of the study was to evaluate the sensitivity of heating-rate predictions to parametric uncertainties and to differences in methodology. Principal areas of sensitivity which were evaluated include trajectories, angle of attack, thermal protection system (TPS) tile catalycity, nose radius/surface pressure distributions, and viscous interactions. Other areas of concern include thermodynamic/transport properties, wall-temperature variations, and gas cap radiation-prediction methods. The relative importance of each of these effects on AFE heating rates using the boundary-layer integral matrix procedure (BLIMP) program is discussed, and sample results for several of the sensitivity parameters are presented. The most important contribution to the heating rate was determined to be the catalytic wall recombination coefficient, with about a 10 W/cm^2 or 25% deviation from the standard.

Nomenclature

BET	= best estimate trajectory
C_p	= specific heat at constant pressure
h	= altitude; also enthalpy
k	= thermal conductivity
M	= Mach number
m	= vehicle mass
p	= pressure
q	= heating rate
R	= radius
Re	= Reynolds number
S	= streamwise distance from stagnation point
T	= temperature
t	= time
V	= velocity
α	= angle of attack
γ'	= catalytic recombination coefficient
ϵ	= emissivity
μ	= viscosity
ρ	= density

Subscripts

BL	= boundary layer
C	= Cheng
CONV	= convection
FC	= fully catalytic
N	= nose
NC	= noncatalytic
RAD	= radiation
RE	= radiation equilibrium
S	= shock
SL	= shock layer
STAG	= stagnation
w	= wall
∞	= freestream

Presented as Paper 89-1733 at the AIAA 24th Thermophyics Conference, Buffalo, NY, June 12-14, 1989; revision received May 14, 1990; accepted for publication May 15, 1990.

*Senior Advanced Systems Specialist. Senior Member AIAA.
†Principal Engineer. Member AIAA.
‡Associate Engineer; currently with Barnes & Reinecke, Inc.
§Computer Systems Analyst.
¶AFE Project Area Manager.
**Chairman, AFE Aerothermodynamics Panel. Associate Fellow AIAA.

Introduction

THE Shuttle Orbiter-launched aeroassist flight experiment (AFE) (shown in the three-view sketch of Fig. 1) is designed to gather important experimental flight data during a simulated atmospheric encounter comparable to that of an aeroassisted space transfer vehicle (ASTV) returning from geosynchronous Earth orbit (GEO). Like the full-scale ASTV, the 4.3-m-diam AFE will perform an aerobrake maneuver in the Earth's upper atmosphere so that the appropriate velocity decrement is achieved to place the spacecraft in low orbit. This aerobraking maneuver will thus reduce the propellant and vehicle weights compared to an all-propulsive maneuver.

The aerothermodynamic design of the aerobrake component of the AFE is critical because it is desired to use existing Shuttle Orbiter technology in the thermal protection system (TPS) design [i.e., fibrous refractory composite insulation (FRCI-12) tiles on the skirt and cone and Lockheed insulation (LI-2200) tiles on the ellipsoid section]. Because of higher initial entry velocities of the AFE (10 km/s) compared to the Orbiter (7.5 km/s), the heating rates to the aerobrake surface will be higher. Hence, it is desired to have an accurate prediction of these heating rates, which in turn determine the surface temperatures on the vehicle.

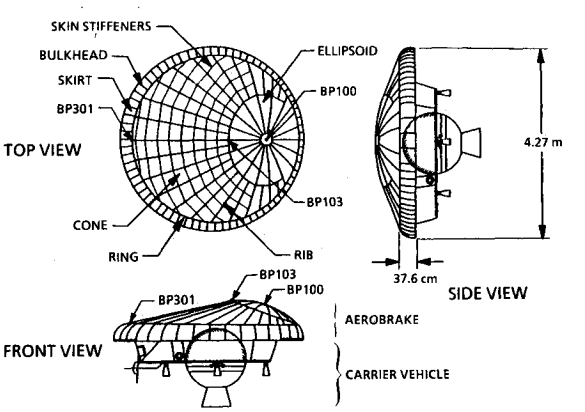

Fig. 1 AFE vehicle configuration.

Several three-dimensional computer codes (e.g., Refs. 1 and 2) have been developed that can solve the Navier-Stokes equations for nonequilibrium flow around the AFE vehicle. Even so, these programs have been used only for point calculations in trajectories and are very time consuming to run. On the other extreme are the simplified methods[3,4] such as those used with the miniature version aeroheating program (MINIVER).[5] These simplified methods are quite suitable for parametric studies, but they do not integrate across the boundary layer or shock layer, and they assume constant wall catalycity.

As a result, a compromise was made where a two-layer (inviscid/viscous) approach was used to conduct the current study and produce the AFE aerothermodynamic data book.[6–8] With this approach, an axisymmetric boundary-layer program, BLIMP,[9] was used with input from an inviscid axisymmetric Euler solution (BLUNT2D)[10] for the pressure distributions, together with geometric metric coefficients. The boundary-layer program provided the capability for modeling a multicomponent, chemically reacting gas using an integral matrix procedure to solve the nonsimilar boundary-layer equations. Temperature-varying wall catalycity options were used with BLIMP for various trajectories in this AFE heating sensitivity study as described in the following sections.

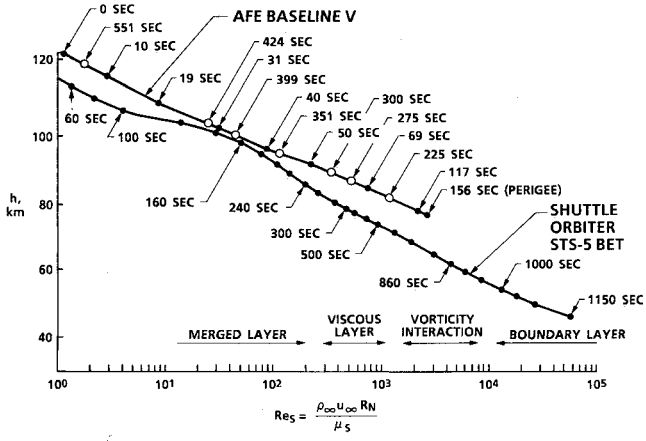

Fig. 2 Trajectory values of altitude and Re_s.

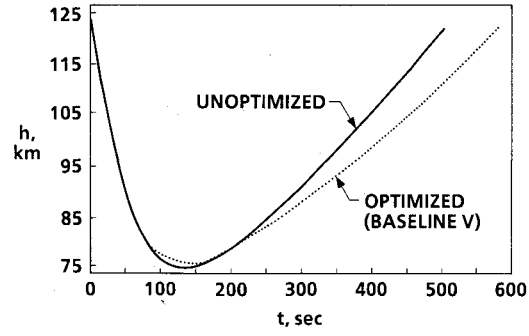

Fig. 3 Altitude vs entry time for AFE trajectories.

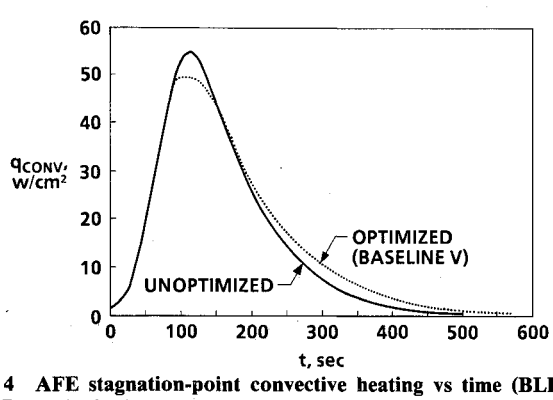

Fig. 4 AFE stagnation-point convective heating vs time (BLIMP-FC, R_N = 2.53 m).

Analysis and Results

Trajectory

Possibly the most important parameter on which the heating rate is dependent is the entry trajectory. For example, during the latter part of the Shuttle Orbiter entry trajectory, the altitudes and high heating rates occur in the continuum or boundary-layer regime as seen in Fig. 2 (from Ref. 11). However, the AFE will never fully enter this regime because its perigee is only about 75 km, which lies in the middle of the vorticity interaction regime. The altitudes for these two trajectories are plotted as a function of Re_s in Fig. 2, with the flow regimes defined from Ref. 12.

Since the convective heating rate q_{CONV} is directly proportional to the square root of freestream density, a vehicle trajectory with a lower perigee will have a higher density (or stagnation pressure) and consequently a higher q_{CONV}. This lower altitude usually is a result of a heavier vehicle. However, it is possible at a fixed vehicle mass to decrease the entry angle, change the guidance, and decrease q_{CONV} as obtained with the 1864-kg (4100-lb) AFE-optimized (baseline V) nominal trajectory. If additional trajectory uncertainties are considered, such as a 3σ trajectory, then the maximum heating rates increase with respect to the nominal trajectory.

Comparisons of the 1864-kg AFE-optimized and original (unoptimized) nominal trajectories are shown in the altitude-time plot of Fig. 3. A higher perigee results for the optimized (baseline V) trajectory, as seen in this figure. The corresponding BLIMP stagnation-point heating rates for a fully catalytic wall (approximating equilibrium flow conditions) are shown in Fig. 4 for a 2.53-m (8.3-ft) nose radius for both trajectories. The trajectory optimization produced a 10% reduction in the peak stagnation-point heating rate for this case. The fully catalytic wall BLIMP heating-rate distributions along the AFE pitch plane are presented in Fig. 5. These BLIMP calculations use the BLUNT2D pressure distribution[10] at time-of-peak heating and show about a 10% reduction in q_{CONV} at the stagnation point for the optimized trajectory.

The effect of changing the mass of the AFE from 1243 to 1864 kg (2734 to 4100 lb) on the peak value of q_{CONV} is shown in Fig. 6. The BLIMP program was used for a fully catalytic wall with both a boundary-layer option and a shock-layer option (discussed later). The peak heating rates shown in this figure can be written as a function of the vehicle mass to approximately the one-half power. Increasing the vehicle mass from 1243 to 1864 kg results in an increase of 24% in q_{CONV} for the fully catalytic wall case.

The heating-rate sensitivities due to trajectory dispersion (aerodynamics, atmosphere, c.g., etc.) were presented in Ref. 13, the original paper on which this article is based. Increases in q_{CONV} at three body points (BP), (BP100, BP103, and

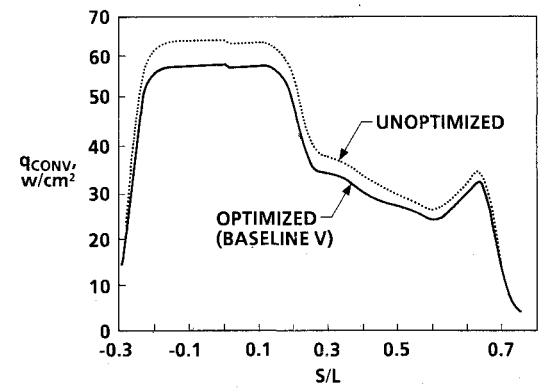

Fig. 5 Convective heating along AFE pitch plane at time-of-peak heating (BLIMP-FC, BLUNT2D pressure distribution).

Table 1 Heating-rate uncertainty and methodology evaluation for AFE Aerobrake

		Convective heating rate			
Type[a]	Description	Δq, W/cm^2	$\Delta q/q_{std}$, %[b]	Standard method	Deviation from standard
U	Trajectory	3.5	9.1	Nominal baseline V	3σ baseline V
U	Angle of attack	3.4	8.8	$\alpha = 0$	$\alpha = -3$ deg
U	Wall catalycity	9.6	24.9	Stewart catalytic wall	Nondecreasing cat.
M	Pressure distribution nose radius	−1.5	−3.8	BLUNT2D pressure distribution	Nose radius = 2.16 m
M	Viscous interaction	1.8	4.7	BLIMP boundary layer	BLIMP shock layer
M	Thermodynamic properties	0.023	0.1	JANNAF Tables	Gupta curvefits
M	Transport properties	1.7	4.4	B/W and M/S properties	Gupta curvefits
M	Wall temperature	2.4	6.1	Rad. eq. temp. with GCR	Rad. eq. temp. without GCR
		Gas cap radiative heating rate			
Type[a]	Description	Δq, W/cm^2	$\Delta q/q_{std}$, %[c]	Standard Method	Deviation from standard
U	Trajectory	1.24	17.6	Nominal baseline V	3σ baseline V
M	Correlation	−2.89	−41.3	Jones/Park	QRAD

[a]U = Uncertainty, M = Methodology. [b]q_{std} = 38.79 W/cm^2. [c]q_{std} = 7.01 W/cm^2.

Note: $q_{max} = (q_{std} + \Sigma M)(1 + U_{RSS}) = (38.79 + 4.4)(1 + \sqrt{.091^2 + .088^2 + .249^2}) + (7.01 - 2.89)(1 + 0.176) = 60.14$ W/cm^2 for $T_{RE} = 1879$ K.

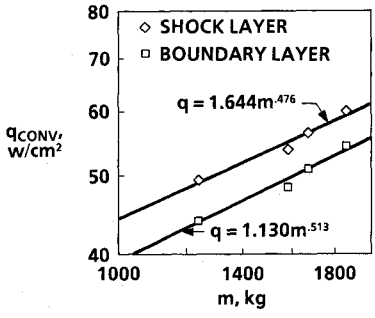

Fig. 6 Maximum convective heating as a function of entry mass (BLIMP-FC, R_N = 2.53 m, unoptimized trajectories).

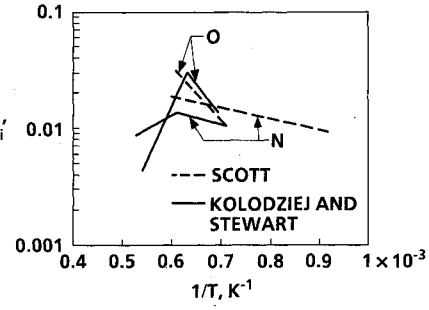

Fig. 7 RCG-coating recombination coefficients.

BP301, defined in Fig. 1) for the 1864-kg AFE optimized 3σ trajectory were about 10% above those for the corresponding nominal trajectory.[13]

At the point of peak heating (114 s from entry interface) during the nominal optimized trajectory, the stagnation-point convective heating rate was predicted to be 38.79 W/cm^2. For the 3σ trajectory, this value increased to 42.33 W/cm^2 (Ref. 13), a 9.1% increase. Table 1 summarizes this and other sensitivities on the nominal stagnation-point heating rates. The parameters, such as trajectory dispersions, have been categorized as uncertainties and/or as methodological differences in predicting heating rates. The nominal, or standard parameter/methodology, and the deviation are tabulated along with the uncertainty on increment in heating rate, referenced to the nominal convective or radiative heating rates.

Angle of Attack

The maximum angle-of-attack uncertainty of the AFE is about 3 deg due to uncertainties associated with the vehicle aerodynamics and center of mass. Previous calculations[1] indicate that the AFE stagnation heating rate increases about 1.1 W/cm^2 per degree of α or about a 7–10% increase above the $\alpha = 0$ heating rate. A 3-deg uncertainty in α results in a peak-stagnation-point convective heating increase of 3.4 W/cm^2 or 8.8% above the nominal value of 38.79 W/cm^2, as seen in Table 1.

Wall Catalycity

Analyses and tests have shown that the catalytic characteristics of the reaction cured glass (RCG)-coated tiles on the TPS surface have a major impact on surface heating for nonequilibrium flows. Because of the desire to maintain the aerobrake tile temperatures less than 1867 K (2900°F) to protect surface experiments, it is important that the tile catalycity be defined as accurately as possible.

Early estimates of the partially catalytic to fully catalytic heating ratio q/q_{FC} of 0.6 were found to be too low when compared to arcjet test data that were curvefit and input into BLIMP. One arcjet datum curvefit as a function of temperature was obtained for T_w up to 1670 K by Scott.[14] A later set of arcjet data was obtained by Kolodziej and Stewart[15] at Ames Research Center for T_w up to 1905 K. An interesting feature of this latter data was that the nitrogen and oxygen recombination coefficients γ_i' tended to decrease at T_w above 1580 and 1640 K, respectively. The γ_i' data obtained from both of these tests are plotted in Fig. 7, showing the change in slope of the Ref. 15 data.

The effect of wall catalycity is seen in Fig. 8 as a function of time for an 2.53-m AFE nose radius. This figure shows the stagnation-point BLIMP heating rates for the fully catalytic wall and a partially catalytic wall using extrapolations of Scott's[14] curvefits and the Kolodziej and Stewart's[15] curvefits. In the lower T_w range between 0–60 s and 190–400 s of the trajectory, the value of q_{CONV} is practically the same for the two sets of recombination rates. However, using the higher T_w catalycity relations of Ref. 15, q_{CONV} decreases significantly during the period of 60–190 s. The corresponding ratio of q/q_{FC} is plotted as a function of time in Fig. 9. At peak heating, this figure shows a value of 0.95 for the Ref. 14 extrapolated data, but only 0.77 for the Ref. 15 curvefits. The values of q/q_{FC} change slope at 60 and 190 s, as the data in Fig. 7 changes slope at the corresponding T_w.

A plot of q_{CONV} around the AFE pitch plane for a fully catalytic wall, partially catalytic wall (based on Ref. 15), and a noncatalytic wall is presented in Fig. 10. This distribution was computed with BLIMP using the pressure ratio distribution from an inviscid Euler solution.[10] There is a significant difference in heating rate at the stagnation point (32%) between the fully catalytic heating rate and the partially catalytic heating rate using the high-T_w curvefits.[15] In the region of the low-T_w catalytic equations ($S/L > 0.4$), these heating rates are closer

together. The noncatalytic wall heating rate is significantly lower (41%) than the partially catalytic heating rate at the stagnation point. At this point, the partially catalytic/fully catalytic ratio is 0.68 compared to a value of 0.38 for the noncatalytic/fully catalytic ratio.

Since the heating rate is so sensitive to wall catalycity effects, a conservative approach to the uncertainty in the variation of catalycity with T_w is to assume that the catalycity does not decrease with increasing T_w but remains constant at the peak value. Thus, γ'_N would remain constant for $T_w > 1640$ K, and γ'_O would be assumed constant for $T_w > 1580$ K. Using these modified catalycity relations, the BLIMP computed value of q_{CONV} increased from 38.79 W/cm^2 to 48.46 W/cm^2 at the stagnation point, a 24.9% increase, as shown in Table 1.

Nose Radius/Pressure Ratio Distribution

The method of determining the velocity gradient can have a significant effect on the heating at the stagnation point. Two methods are compared here. One uses an effective radius of curvature and Newtonian pressure distribution, whereas the other uses an input pressure distribution from an Euler solution.

It can be seen in Fig. 4 that the peak stagnation-point heating rates for the optimized (baseline V) nominal AFE trajectory are lower than those in Fig. 5. Similarly, the peak values in Fig. 8 for the same trajectory are lower than those in Fig. 10. The values in Figs. 4 and 8 used a fixed nose radius of 2.53 m, whereas those in Figs. 5 and 10 used a pressure distribution from an axisymmetric inviscid Euler solution.[10]

The resulting differences in stagnation-point heating show the effect of computing the stagnation-point velocity gradient by different methods. The use of the Euler pressure distribution was expected to produce higher heating rates since the ellipsoidal AFE nose is not axisymmetric. It has a larger radius of curvature in the yaw plane than in the pitch plane. A more recent effective nose radius derived from a three-dimensional Navier-Stokes solution[1] was obtained by using an axisymmetric viscous shock-layer (VSL) solution[16] that could produce the same stagnation-point heating rate as the three-dimensional solution. This radius inferred from heat-flux calculations was determined to be 2.16 m (7.1 ft)[7] (compared to that of 2.53 m used for the earlier AFE studies). When $R_N = 2.16$ m was used with BLIMP (without the pressure distribution), the resulting heating rates decreased 3.8% from those with the pressure distribution. This value is listed as a negative change in Table 1 and as a change in the methodology (rather than an uncertainty).

Other effects of pressure distribution were assessed in the previous AFE sensitivity analysis.[13] These included pressure distributions performed at higher altitude (around 87 km for the descending and ascending part of the trajectory), which were only slightly different than the distribution at peak heating. These values of P/P_{STAG}, which were all performed at zero angle of attack, resulted in a negligible difference in heating rate.

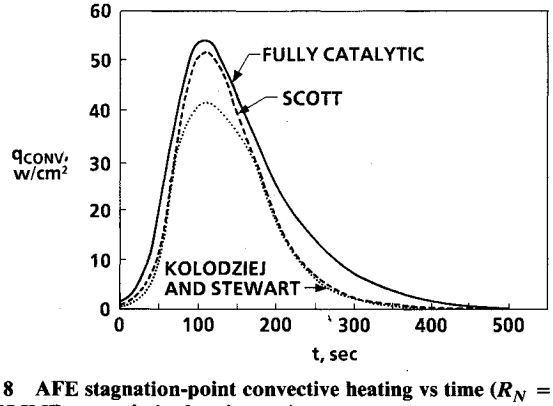

Fig. 8 AFE stagnation-point convective heating vs time ($R_N = 2.53$ m, BLIMP, unoptimized trajectory).

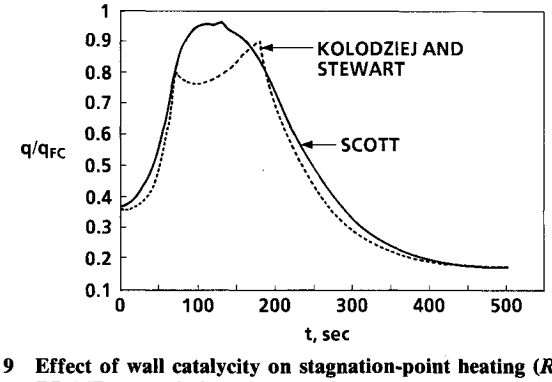

Fig. 9 Effect of wall catalycity on stagnation-point heating ($R_N = 2.53$ m, BLIMP, unoptimized trajectory).

Viscous Interaction

Viscous effects are important in the lower density (higher altitude) regimes where Re_s is of the order of 10^4 or lower (see Fig. 2) and the boundary layer grows to become a significant portion of the shock layer. Cheng[17] has described the effects of viscous interactions on heating rates by plotting the ratio of shock-layer to boundary-layer heating rates as a function of a Reynolds number Re_C and comparing with test data as shown in Fig. 11. Heating-rate ratios q_{SL}/q_{BL} have been computed by BLIMP for the Orbiter STS-5 entry trajectory and AFE nominal baseline V trajectory and are included in Fig. 11. The heating rates were computed assuming chemical equilibrium and by using a shock-layer option in BLIMP. This option solves the boundary-layer equations across the shock layer. The resulting q_{SL}/q_{BL} ratio follows the general trend of the other results in Fig. 11 and shows an approximately 10% increase in heating rates above the boundary-layer analysis values.

In Fig. 6, a comparison was made between the BLIMP-predicted shock-layer and boundary-layer stagnation-point heating rates as a function of vehicle mass at the time-of-peak heating for a fully catalytic wall using $R_N = 2.53$ m. The increase in heating predictions of the shock-layer over the boundary-layer methods ranges from 10–12% as m changes from 1243 to 1864 kg, respectively. At the time-of-peak heating during the AFE baseline V nominal trajectory, the BLIMP shock-layer option was used to compute a stagnation-point heating rate for a partially catalytic wall using Ref. 15 curvefits. As shown in Table 1, the heating increased 4.7% over the corresponding boundary-layer value.

A comparison of stagnation-point heating results with two VSL analyses, the Miner and Lewis code[18] and BLIMP, is presented in Fig. 12 as a function of R_N from 0.305 to 2.53 m for a partially catalytic wall using the curvefits of Ref. 15. Also shown is the result from the VSL analysis of Gupta et al.[19] for a 2.29-m nose radius. The Gupta result is about 6% higher than the BLIMP values, which are about 13% higher than the

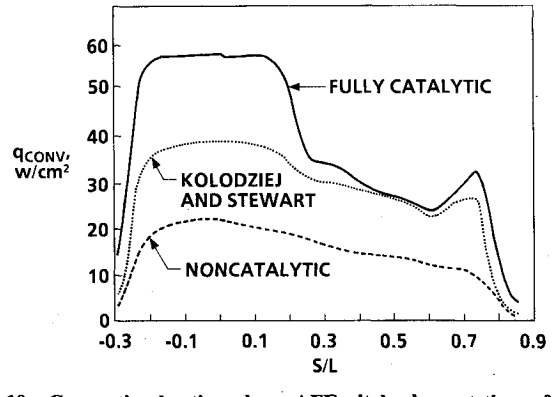

Fig. 10 Convective heating along AFE pitch plane at time-of-peak heating (BLIMP, BLUNT2D pressure distribution, baseline V trajectory).

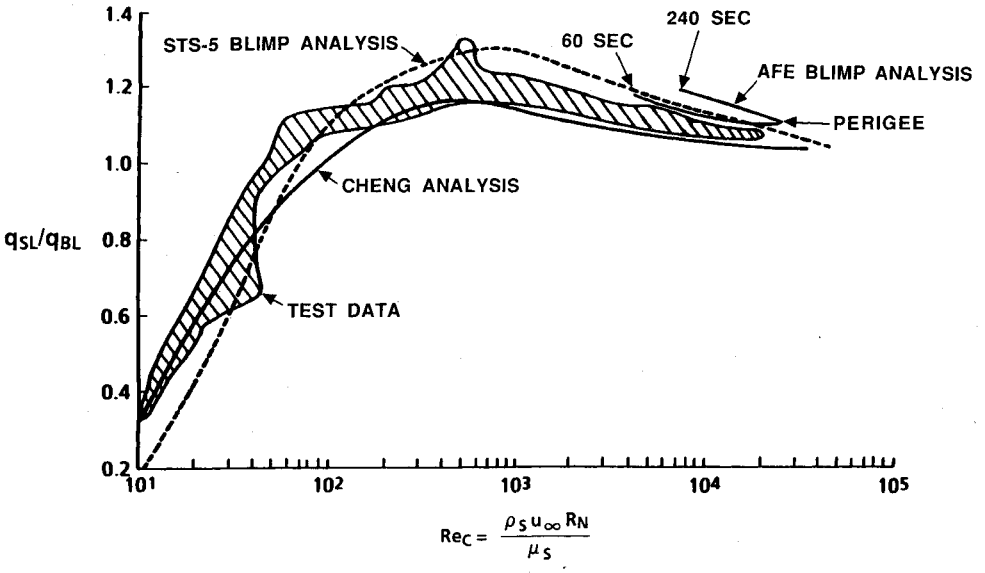

Fig. 11 VSL to BL equilibrium heating ratio vs Re_C.

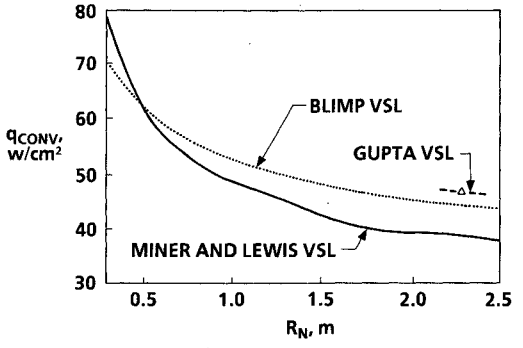

Fig. 12 Convective heating vs nose radius (VSL analyses, Kolodziej/Stewart wall catalycity, unoptimized trajectory).

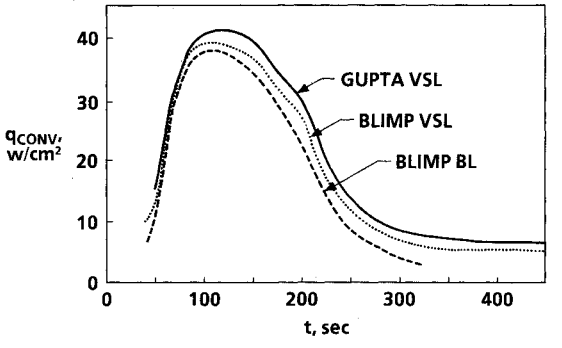

Fig. 13 AFE stagnation-point convective heating vs time (R_N = 2.16 m, Kolodziej/Stewart wall catalycity, baseline V trajectory).

Miner and Lewis values. Some of this disparity may be due to differences in thermodynamic and/or transport properties (discussed later) between the three programs.

Figure 13 presents a plot of the AFE stagnation-point heating rate obtained with three methods: 1) Gupta VSL prediction, 2) BLIMP shock-layer option, and 3) BLIMP boundary-layer option, as a function of time for the baseline V nominal trajectory. For all of these analyses, the nose radius was taken as 2.16 m. The ratio of the two lower curves was shown as a function of Re_C in Fig. 11. In the two shock-layer curves of Fig. 13, the effects of finite shock thickness and wall slip are not taken into account. These effects should not significantly influence the calculated heating for altitudes below 90 km; however, above 90 km, these slip effects should be included,[7] as the two shock-layer curves in this figure remain fairly flat without these effects considered.

Thermodynamic/Transport Properties

Some of the differences in q_{CONV} between the Gupta VSL and BLIMP shock-layer methods shown in Fig. 12 may be attributed to differences in the thermodynamic and/or transport properties used in the two programs. The thermodynamic properties used by Gupta et al.[19] are valid to 30,000 K, whereas the properties provided by the JANNAF tables and used in the BLIMP code[20] are valid only to 6000 K. A comparison of the atomic oxygen and nitrogen specific heat and enthalpy as a function of temperature for the two data sets was presented in Ref. 13. For temperatures above 6000 K, BLIMP uses the JANNAF data extrapolated to 30,000 K. At the lower temperatures near the wall, the values of C_p and h differ little from method to method. At high temperatures that occur near the shock wave, the properties are considerably different. However, replacing the JANNAF tables in the BLIMP input with the thermodynamic properties used by Gupta resulted in a negligible change in q_{CONV} (0.1%) as seen in Table 1.

A comparison of thermal conductivity as computed by BLIMP[20] and by Gupta's curvefits[19] was presented in Ref. 13 as a function of temperature. At the stagnation point, at time-of-peak heating in the AFE baseline V nominal trajectory, the Gupta value of k_w was 17.1% above that of BLIMP, and the corresponding value of μ_w was 13.8% above that of BLIMP. The Mason and Saxena and Buddenberg and Wilke relations used by BLIMP to compute k and μ, respectively,[20] were replaced by Gupta's curvefits. The net result of the transport-property sensitivity was an increase in q_{CONV} of 4.4% as seen in Table 1.

Wall Temperature

The BLIMP analyses of q_{CONV} used a value of T_{RE} for the wall temperature that was achieved through an iteration process until the input and output values of T_w converged. This temperature is based on a value of ϵ_w = 0.85 for the RCG-coated tiles. In the early BLIMP analyses of heating to the AFE aerobrake, after T_w converged, the gas cap radiative heating was simply added to q_{CONV} to produce the total heating rate. However, T_w actually depends on the sum of the two heating components, which is higher than the T_w for convective heating alone. When this higher T_w is incorporated into BLIMP in an iterative fashion, the convective heating rates were reduced. This reduced value is the nominal heating rate. As shown in Table 1, the heating rate increases 6.1% if the earlier methods are used.

Figure 14 shows the influence of T_w on q_{CONV} as obtained with the BLIMP boundary-layer option. For equilibrium

flow, there is only a slight variation in q_{CONV} with T_w. However, for the nonequilibrium flow cases, the variation of q_{CONV} is highly dependent on the wall catalycity (and hence on T_w). The high T_w catalycity curve using Ref. 15 curvefits shows q_{CONV} decreasing with T_w, whereas q_{CONV} increases with T_w for the low-T_w catalycity relations.[15] These trends correspond to the decrease or increase in γ_i' with T_w as presented in Fig. 7. The intersection of the T_{RE} curve with the high-T_w catalycity curve shows q_{CONV} without including gas cap radiation (GCR). The symbol on the curve shows the 6.1% drop in q_{CONV} with this radiative heating effect included in the value of T_w.

Gas Cap Radiation

The gas cap radiation-prediction method currently used for the AFE aerothermodynamic data book[6-8] is based on a correlation by Jones[21] of Park's detailed line-by-line nonequilibrium radiation calculations.[22] A simple program, termed GASRAD, was written to compute the stagnation-point radiative heating using Jones' correlation as a function of altitude, V_∞, ρ_∞, and R_N. Currently, the 2.29-m (7.5-ft) geometric radius is being used for the AFE stagnation-point heating.

An additional gas cap radiation analysis was performed for the AFE aerobrake. This method was based on a modification of the QRAD program that provided excellent agreement with Apollo command module (CM) flight data.[23] This program uses the four-band (IR lines, visible continuum, UV lines, UV continuum) equilibrium air radiation model with absorption coefficients curvefitted from data by Page et al.[24] In addition, the method of Ref. 23 used a binary scaling (velocity-dependent) relation based on a collision-limiting approximation for nonequilibrium radiation, plus included the effects of nonadiabatic flow, three-dimensional geometry, and truncation.

Figure 15 presents the differences between the predicted AFE stagnation-point radiative heating using the Jones/Park and QRAD methods for a 2.29-m nose radius for the baseline V nominal trajectory. Some of this discrepancy can be attributed to the fact that there is no radiative cooling or three-dimensional effects incorporated into the Jones/Park method and the fact that the QRAD program uses absorption coefficient data extrapolated from 0.1 atm to AFE values (peak of 0.03 atm). An additional data point is shown on this chart. This point was obtained from the Radiating, Inviscid Flow, Stagnation-Point (RIFSP) program of Sutton[25] for equilibrium air with an added component of nonequilibrium radiation obtained from the QRAD program. The resulting point is higher than the QRAD results, but still significantly lower than the Jones/Park results. To be conservative, it was decided to use the Jones/Park method for the data book. It is hoped that some of this discrepancy will be resolved in the flight test of the AFE radiative heating experiment.

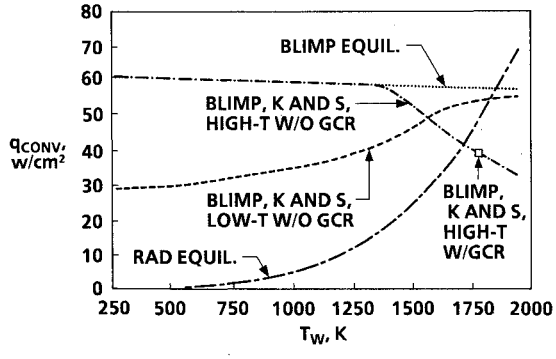

Fig. 14 AFE stagnation-point convective heating vs wall temperature (BLIMP, BLUNT2D pressure distribution, baseline V trajectory).

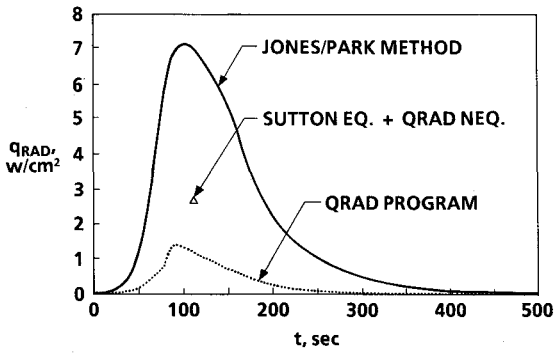

Fig. 15 AFE stagnation-point convective heating vs time (R_N = 2.29 m, baseline V trajectory).

In Table 1, the radiative-heating sensitivity analysis is treated separately from the convective-heating sensitivity analysis. The uncertainty in the trajectory results in a 17.6% difference in heating rates between the 3σ and nominal trajectories using the Jones/Park method. Because of the large disparity between the Jones/Park and QRAD methods, an average value between the two was considered more reasonable, and the −41.3% deviation from the standard (i.e., Jones/Park) reflects this value.

Conclusions

The relative importance of each of the AFE aerobrake heating sensitivities to various parameters has been presented. The standard calculation for this study was to use the nominal baseline V trajectory at $\alpha = 0$ using the catalytic wall recombination coefficient curvefits of Ref. 15, with an axisymmetric Euler inviscid surface pressure distribution[10] with the BLIMP boundary-layer option. Radiation equilibrium temperature with the gas cap radiative heating used in the T_w iteration was considered. The convective-heating calculations used the JANNAF thermodynamic tables, and Mason/Saxena and Buddenberg/Wilke transport properties, with the Jones/Park method of computing q_{RAD}. This produced the standard heating rates of q_{CONV} = 38.8 W/cm² (34.2 Btu/ft² s), q_{RAD} = 7.0 W/cm² (6.2 Btu/ft² s), and q_{TOTAL} = 45.8 W/cm² (40.4 Btu/ft² s).

The highest value of deviation from the standard of all of the sensitivities was the wall catalycity at 9.6 W/cm² (24.9%). Although this percentage was lower than the deviation from the radiation methodology (−41.3%), the radiative heating component is much lower than that of convection. A maximum total heating rate was computed by adding the root-sum-square of all uncertainties to the sum of deviations due to changes in methodology. The resulting q_{TOTAL} is 60.1 W/cm², a 31.2% increase over the standard. Although this translates to an 1880 K (2924°F) value of T_{RE} (which is slightly higher than the single mission limit for LI-2200 tiles of 1867 K), with conduction losses accounted for, it is expected that the tile temperatures will remain under this single mission limit.

The results of this study are being used to update the aerothermodynamic data book, and they will aid the AFE principal investigators and thermal analysts in the design of the flight experiments and aerobrake TPS.

References

[1]Gnoffo, P. N., and Greene, F. A., "A Computational Study of the Flowfield Surrounding the Aeroassist Flight Experiment Vehicle," AIAA Paper 87-1575, June 1987.

[2]Li, C. P., and Wey, T. C., "Numerical Simulation of Hypersonic Flow Over an Aeroassist Flight Experiment Vehicle," AIAA Paper 88-2675, June 1988.

[3]Detra, R. W., Kemp, N. N., and Riddell, F. R., "Addendum to 'Heat Transfer to Satellite Vehicles Reentering the Atmosphere,'" *Jet Propulsion*, Vol. 27, No. 12, 1957, pp. 1256-1257.

[4]Fay, J. A., and Riddell, F. R., "Theory of Stagnation-Point Heat Transfer in Dissociated Air," *Journal of Aero/Space Sciences*, Vol. 25, No. 2, 1958, pp. 73-85.

[5]Hender, D. R., "A Miniature Version of the JA70 Aerodynamic Heating Computer Program, H800 (MINIVER)," McDonnell Douglas MDC G0462, June 1970, revised Jan. 1972.

[6]Ting, P. C., Rochelle, W. C., Mueller, S. R., Colovin, J. E., Scott, C. D., and Curry, D. M., "Development of AFE Aerobrake Aerothermodynamic Data Book, AIAA Paper 89-1734, June 1989.

[7]Rochelle, W. C., Ting, P. C., Mueller, S. R., and Colovin, J. E., "Data Book Documentation, AFE Aerobrake Aerothermodynamic Data Book for Baseline V Trajectory, Vol. I: Pitch Plane," Lockheed Engineering & Sciences Co., LESC-26950 (JSC-23623), April 1989.

[8]Ting, P. C., and Rochelle, W. C., "Data Book Documentation, AFE Aerothermodynamic Data Book for Baseline V Trajectory, Vol. II: Off-Pitch Planes," Lockheed Engineering & Sciences Co., LESC-26950 (JSC-23623), Sept. 1989.

[9]Murray, A. L., "Further Enhancements of the BLIMP Computer Code and User's Guide," Air Force Wright Aeronautical Lab., Wright-Patterson AFB, OH, AFWAL-TR-88-3010, June 1988.

[10]Hamilton, H. H., and Spall, J. R. "Time-Dependent Solution for Axisymmetric Flow Over a Blunt Body with Ideal Gas, CF_4, or Equilibrium Air Chemistry," NASA TM 87675, July 1986.

[11]Ting, P. C., Rochelle, W. C., and Curry, D. M., "Comparison of Viscous Shock Layer and Boundary-Layer Re-entry Heating Techniques for Orbiter Nose Cap," AIAA Paper 86-1350, June 1986.

[12]Blottner, F. G., "Viscous Shock Layer at the Stagnation Point with Nonequilibrium Chemistry," *AIAA Journal,* Vol. 7, No 12, 1969, pp. 2281–2288.

[13]Rochelle, W. C., Ting, P. C., Mueller, S. R., Colovin, J. E., Bouslog, S. A., Curry, D. M., and Scott, C. D., "Aerobrake Heating-Rate Sensitivity Study for the Aeroassist Flight Experiment (AFE)," AIAA Paper 89-1733, June 1989.

[14]Scott, C. D., "Catalytic Recombination of Oxygen and Nitrogen in High-Temperature Reusable Surface Insulation," *Aerothermodynamics and Planetary Entry,* Vol. 77, Progress in Astronautics and Aeronautics, AIAA, New York, 1981, pp. 192–212.

[15]Kolodziej, P., and Stewart, D. A., "Nitrogen Recombination on High-Temperature Reusable Surface Insulation and the Analysis of its Effects on Surface Catalysis," AIAA Paper 87-1637, June 1987.

[16]Gupta, R. N., and Simmons, A. L., "Stagnation Flowfield Analysis for an Aeroassist Flight Experiment Vehicle," AIAA Paper 88-2613, June 1988.

[17]Cheng, H. K., "The Blunt Body Problem in Hypersonic Flow at Low Reynolds No.," Cornell Aeronautical Lab., Buffalo, NY, Rept. AF-1285-A-10, June 1963.

[18]Miner, E. W., and Lewis, C. H., "Hypersonic Ionizing Air Viscous Shock Layer Flows over Nonanalytical Blunt Bodies," NASA CR-2550, May 1975.

[19]Gupta, R. N., Yos, J. M., and Thompson, R. A., "A Review of Reaction Rates and Thermodynamic and Transport Properties for the 11-Species Air Model for Chemical and Thermal Nonequilibrium Calculations to 30,000 K," NASA TM-101528, Feb. 1989.

[20]Deblaye, C., and Bartlett, E. P., "An Evaluation of Thermodynamic and Transport Properties for Use in the BLIMP Nonsimilar Multicomponent Boundary-Layer Program," Sandia Lab., Albuquerque, NM, SC-CR-69-3271, July 1969.

[21]Hamilton, H. H., Gupta, R. N., and Jones, J. J., "Flight Stagnation-Point Heating Calculations on Aeroassist Flight Experiment Vehicle," *Journal of Spacecraft,* Vol. 28, No. 1, 1991, pp. 125–128.

[22]Park, C., "Assessment of Two-Temperature Kinetic Model for Ionizing Air," AIAA Paper 87-1574, June 1987.

[23]Ried, R. C., Rochelle, W. C., and Milhoan, J. D., "Radiative Heating to the Apollo Command Module: Engineering Prediction and Flight Measurement," NASA TM X-58091, April 1972.

[24]Page, W. A., et al., "Radiative Transport in Inviscid Nonadiabatic Stagnation-Region Shock Layers, AIAA Paper 68-784, June 1968.

[25]Sutton, K., and Hartung, L. C., "Equilibrium Radiative Heating Tables for Earth Entry," NASA TM-102652, May 1990.